



UNIVERSIDADE ESTADUAL DE CAMPINAS  
SISTEMA DE BIBLIOTECAS DA UNICAMP  
REPOSITÓRIO DA PRODUÇÃO CIENTÍFICA E INTELLECTUAL DA UNICAMP

**Versão do arquivo anexado / Version of attached file:**

Versão do Editor / Published Version

**Mais informações no site da editora / Further information on publisher's website:**

<https://ieeexplore.ieee.org/document/9127529>

**DOI: 10.1109/TMAG.2020.3005390**

**Direitos autorais / Publisher's copyright statement:**

©2020 by Institute of Electrical and Electronics Engineers. All rights reserved.

DIRETORIA DE TRATAMENTO DA INFORMAÇÃO

Cidade Universitária Zeferino Vaz Barão Geraldo

CEP 13083-970 – Campinas SP

Fone: (19) 3521-6493

<http://www.repositorio.unicamp.br>

# Use of a micromagnetic nondestructive test in the evaluation of the $\alpha'$ -martensitic transformation generated in the mechanical fatigue process of the AISI 304L stainless steel

Roberto M. Giménez C., Freddy A. Franco G., Paula F. S. Farina.

School of Mechanical Engineering, University of Campinas – UNICAMP, 13083-860, Campinas, SP, Brazil.

The detection of the strain-induced martensitic transformation with the Magnetic Barkhausen Noise (MBN) was investigated in the high-cycle fatigue (HCF) of the AISI 304L stainless steel at different points of the surface of an hourglass-type specimen. Load controlled fatigue tests with loads below and above the fatigue limit were performed. Each fatigue test was interrupted at certain numbers of cycles, prior to fracture, and MBN measurements were performed without applied loading. Comparing with the initial condition of the steel under study, no large changes in the MBN measurements were detected in the specimens subjected to loads near the fatigue limit, i.e., no  $\alpha'$ -martensitic transformation was detected. In the specimen subjected to the greatest load, it was possible to detect an uncommon distribution of the MBN signals, which are correlated to the strain-induced  $\alpha'$ -martensite and that were verified with optical microscopy and X-ray diffraction (XRD). The results show that the MBN is a sensitive technique to detect the strain-induced  $\alpha'$ -martensite in HCF tests, which can be used as an indirect parameter to show the fatigue damage of materials.

**Index Terms**—Magnetic Barkhausen Noise, Strain-induced martensitic transformation, High-cycle fatigue, Austenitic stainless steel, Nondestructive testing.

## I. INTRODUCTION

AUSTENITIC stainless steels are widely used in industry, such as in structural components of machines, petrochemical plants, nuclear power plants, pressure vessels, and so on. This is due to their excellent mechanical properties and resistance to corrosion. In many of these applications, the materials are subjected to cyclic loads, which can cause component failure. [3]

Several austenitic stainless steels, e.g., the 304L, are metastable because they can undergo martensitic transformation by cold working. This phenomenon can lead to the transformation of the paramagnetic face centered cubic (fcc) austenite into the ferromagnetic body centered cubic (bcc)  $\alpha'$ -martensite and/or the paramagnetic hcp  $\epsilon$ -martensite. [4]

This transformation can also occur when the material is subjected to cyclical loads. Such transformation can take place in both LCF (low-cycle fatigue) [5], [6] and HCF [7], [8]. Fatigue studies in metastable austenitic stainless steel have shown that martensitic transformation is associated with the amplitude of plastic deformation as well as with the cumulative plastic strain during fatigue testing [6]. It has also been shown that when  $\alpha'$ -martensite is formed, its volumetric fraction increases with the increase of the number of cycles until material failure [5], [6], and that large amounts of  $\alpha'$ -martensite are found in the crack region after fatigue testing [9], [10]. Therefore, monitoring the martensitic transformation in the metastable austenitic steels can be used as an indirect parameter of fatigue damage of materials in work [9], [11], [12].

Because  $\alpha'$ -martensite is a magnetic phase, it can be detected by nondestructive magnetic techniques. In axial fatigue testing, M. Grosse et al. [9] evaluated the fatigue damage by martensitic transformation in a X6CrNiTi18-10 austenitic

stainless steel by the measurements of magnetic stray field strength and eddy current. Using an hourglass-type specimen they found: a) an increase of the  $\alpha'$ -martensite content with the number of cycles, b) a variable distribution of the  $\alpha'$ -martensite on the specimen. The highest concentration of  $\alpha'$ -martensite was found near the surface and in the crack region of the specimens subjected to the largest number of cycles. M. Lang et al. [11] used the SQUID measuring technique to determine the fatigue damage in an AISI 321 stainless steel by characterization of the  $\alpha'$ -martensite content. They found changes in the magnetic flux density with the number of cycles, which were related to the amount of  $\alpha'$ -martensite formed and the fatigue state of the material.

For the past years, the Magnetic Barkhausen Noise (MBN) has been used as a NDT (nondestructive technique) to evaluate the properties of ferromagnetic materials. The MBN consists of electromagnetic pulses generated in ferromagnetic materials when they are magnetized continuously. It occurs mainly because of the irreversible movement of the magnetic domain walls when the magnetic moments attempt to move in the direction of the applied magnetic field [2]. Internal defects in the material, known as pinning sites, act as a barrier of the domain walls movement until the magnetic field is increased enough to overcome it. When this condition is reached, a small sudden pulse in magnetization occurs. These pulses, known as Barkhausen jumps, generate a discontinuous change in the magnetization, which can be detected with a search coil placed on the material. Because the MBN signal depends on the microstructural properties of ferromagnetic materials, it is often used as a nondestructive technique to evaluate such materials.

Some researchers [13]–[15] have used the MBN technique to evaluate the strain-induced martensitic transformation in austenitic stainless steel subjected to monotonic loads. The

behavior found in many studies is the increase of the MBN signal with the increase in the amount of martensite transformed during plastic deformation. But studies also show that the MBN signal can also be affected by other parameters, such as dislocation density, magnetization direction, texture, stress state, residual stresses, plastic deformation, etc. Thus, the contribution of each parameter to the MBN signal is still under study. In fatigue tests of austenitic stainless steels, only one study using the MBN technique was found. Vincent et. al. [16] investigated the MBN from the strain-induced martensite during the LCF of the AISI 304L steel. They found changes of the MBN signal along the  $\sigma$  versus  $\varepsilon$  loop, showing that the signal is greatly affected by the internal stresses within the martensite. However, measurements at the same point of the  $\sigma$  versus  $\varepsilon$  loop for different numbers of cycles have shown a continuous increase of the MBN signal by the continuous increase in the amount of martensite transformed during fatigue testing. At the end of the fatigue life, the MBN signal decreased because of the formation of cracks in the specimen.

In this study, the Magnetic Barkhausen Noise technique was used to evaluate the  $\alpha'$ -martensitic transformation at different points on the surface of fatigued specimens with different loads and number of cycles. In terms of microstructural characterization, optical microscopy and X-ray diffraction were used in the selected specimens to confirm the correlation of the MBN results with the fatigue state of the material. The results of this research show that the MBN technique has potential in monitoring the martensitic transformation generated in HCF. Thus, it enables the conduction of future researches that deepen the study of the technique application to be able to correlate the behavior of the measured signals with the damage evolution in HCF.

### A. Magnetic Barkhausen Noise

Barkhausen signals are produced by discontinuous variations in magnetization when ferromagnetic materials are subjected to a changing magnetic field. The variations are attributed to alterations in the velocity of magnetic domain walls when domains interact with pinning centers formed by local microstructural material defects such as dislocations, dissolved atoms, vacancies, and phase and grain boundaries. Pinning-center interaction temporarily impedes domain-wall motion until enough external energy is supplied to overcome local energy barriers created by the pinning centers.

Laboratory MBN measuring equipment is based on a probe, consisting of a magnetizing yoke and an MBN pickup coil sensor, both simultaneously in contact with the surface of the sample to be studied [1]. While the yoke generates a magnetic field in the material, the pick-up coil reads a voltage signal induced by the magnetic field after interacting with the material. A schematic representation of an MBN experimental setup is shown in Fig. 4 MBN is not produced uniformly throughout the magnetization cycle but is concentrated in two bursts of activities per excitation cycle near the coercive field (see Fig. 1). The magnetic emissions, in the form of a series of voltage pulses, are detected by a pick-up coil, and are

generated by irreversible and reversible movements of the 180° magnetic domain walls and by the rotation of the magnetic domain [2].

[Fig. 1 about here.]

The fluctuation of the MBN signals is random [2], has to be statistically treated, and therefore many parameters can be calculated. In this study, the following parameters were used to analyze the results. The *Root Mean Square* ( $MBN_{RMS}$ ): The root mean square of the MBN signal ( $MBN_{RMS}$ ) is calculated using Eq. 1, where  $V_i$  represents the instant voltage at a specific time,  $V_m$  is the average voltage value and  $n$  is the number of signal points. The  $MBN_{RMS}$  parameter has Volts units. The *MBN Peak Position*: Is the amplitude of the applied magnetic field relative to the position of the maximum value of the MBN envelope (or MBN signal profile). A smoothing by sliding average method was used for obtain MBN signal profile. (see Fig.1)). And the *MBN Peak Height*, which represents the maximum value of the MBN signal profile.

$$MBN_{rms} = \sqrt{\frac{\sum_i^n (V_i - V_m)^2}{n - 1}} \quad (1)$$

## II. EXPERIMENTAL PROCEDURE

### 1) Materials

The studied material was a commercially available AISI 304L stainless steel supplied by Villares Metals S. A. (Brazil) in the annealed state. Tables I and II show its mechanical properties and chemical composition, respectively. The chemical composition situates the steel in austenite + 5% delta ferrite ( $\delta$ -ferrite) field near the martensite field in the Schaeffler diagram [17], therefore, some amount of  $\delta$ -ferrite is expected in the as-received state. Because the steel is near the martensite field, one can say that it is sensitive to the strain-induced martensite transformation [14].

[TABLE 1 about here.]

[TABLE 2 about here.]

Specimens for the rotative bending fatigue test were machined from the steel bars to an hourglass-shaped specimen with the dimensions shown in Fig. 2 according to the suggested test specimen configurations in the fatigue testing machine instruction manual. All specimens were mechanically polished for eliminating the remaining circumferential notches and imparting a “mirror-like” finish.

[Fig. 2 about here.]

### 2) Magnetic Barkhausen Noise measurement

The MBN sensor consists of a u-shaped FeSi yoke with 350 turns of AWG-28 copper wire to produce the magnetic field in the material. The poles of the yoke were machined with a special geometry to establish better contact with the hourglass fatigue specimens. The MBN signal was measured with a highly sensitive pickup coil, which consists of 3000 turns of AWG-44 copper wire and ferrite core. Fig. 3 shows the experimental setup development for the MBN measurements. A 40-Hz sinusoidal voltage with an amplitude of 0.8 V was

applied to the MBN probe that magnetizes the specimen in the axial direction. The MBN signals collected with the pickup coil were band-pass filtered (1-150 kHz), amplified (30 dB gain), and sampled at 300 kHz.

[Fig. 3 about here.]

The measurements were made in the unloaded condition at points located axially and circumferentially on the specimen surface, as Fig. 4 shows. The measured points were positioned in six circumferential positions with  $60^\circ$  separations between each one. Each circumferential position contains eleven points separated by 1 mm along the axial direction. All the points are geometrically positioned in the central region of the test specimen. Six replicates of MBN signals were collected from each point in the specimen. Finally, the signal was processed on the computer. The well-known parameters Root mean square of the MBN signal ( $MBN_{RMS}$ ), peak position, and peak height of MBN signal profile (relative to the applied voltage) were used. The RMS calculation was made for the MBN signals generated in two complete cycles of magnetization (four MBN bursts), and the MBN signal profile (envelope) was calculated for one burst.

[Fig. 4 about here.]

### 3) Experiment

Four fatigue test specimens were used in this research. One of them was randomly selected and used as an initial condition of the material. The remaining three specimens were subjected to fatigue tests by using a load-controlled rotating cantilever bending fatigue test machine, with a test frequency of 100 Hz. In this type of configuration, the bending moment and the maximum stress (on the surface) along the axial position of the hourglass specimen is nonuniform, as shown schematically in Fig. 5. This allows, in a single fatigue test, different stress levels at different axial positions in a single specimen. Each axial position along a circumference of the specimen is subjected to the same macroscopic stresses and deformations during the tests. The greatest deformations occur on the surface of the specimen in the smallest cross section. Therefore, the martensitic transformation is expected to transform first on the surface and on the subsurface regions of the material near the zero-axial position (see Fig. 4). The tests were carried out in an air-conditioned room with an ambient temperature of  $25^\circ\text{C}$ .

[Fig. 5 about here.]

Loads under and below the classical fatigue limit ( $\approx 230$  MPa) were tested to verify the martensitic transformation. The aim of the tests was to subject the specimens to high numbers of cycles and stop before specimen failure to verify possible martensitic transformations in different points of the specimens' surface after the fatigue tests. The material failure was avoided because it is not possible to correctly magnetize fractured specimens with the projected sensor. This is due to the edge effects that produce a nonuniform magnetization near the edge of the specimen.

For loads above the fatigue limit, the number of cycles for material failure for each test (load) were estimated analytically. Thus, as a means of security, the fatigue tests were stopped in

numbers of cycles lower than those determined analytically. These values are shown in Table III

[TABLE 3 about here.]

After performing the fatigue tests and the MBN measurements, the selected specimens were cut and electropolished in 10%  $\text{HClO}_4$  and 90%  $\text{C}_2\text{H}_4\text{O}_2$  solution at 30 V. To reveal the grains for light microscopic observation, chemical etching was used for 7 s in a mixed solution of 80 ml distilled water, 20 ml HCl, and 0.5 g potassium metabisulfite. The polished specimens were also analyzed by X-ray diffraction using the Philips X'pert Pro MRD XL equipment with  $\text{Co-K}\alpha$  radiation over the range  $45^\circ < 2\theta < 115^\circ$  at 40 KV, 45 mA,  $0.02^\circ$  step size and time per step of 3 s.

## III. RESULTS

### A. Initial microstructure

Figs. 6a and 6b show the optical microscopy of the AISI 304L in the as-received condition for the material cut cross-sectionally and longitudinally, respectively. As expected, small amounts of delta ferrite can be observed. In the cross section, the delta ferrite is found near the austenite grain boundaries, and in the longitudinal section, it is more obviously observed in an elongated form.

[Fig. 6 about here.]

### B. MBN measurements

[Fig. 7 about here.]

Figs. 7a, b, and c represent the  $MBN_{RMS}$  distribution and the MBN envelope of the regions of highest  $MBN_{RMS}$  variations for the specimens S1, S2, and S3, respectively. In each specimen, specific regions with small amplitude of the  $MBN_{RMS}$  can be noted. Little variation of the RMS distribution between these specimens can also be observed. For S1 (initial condition), the circumferential position  $60^\circ$  shows small changes in the  $MBN_{RMS}$  value. The MBN envelope of the eleven points in such line shows that all peak positions are at approximately 0.15 V, with small peak amplitude values. Similar phenomena are observed for S2 and S3.

The  $MBN_{RMS}$  distribution for the S4 specimen (Fig. 8) shows high variations of the RMS value in certain circumferential positions. The Fig. 8 also shows the orientation of the load in the specimen, which is also valid for Fig. 7. More measurements in the circumferential direction were taken on this specimen to generate a higher resolution of the amplitude distribution of MBN signals. In some circumferential positions ( $60^\circ$ - $150^\circ$ ),  $MBN_{RMS}$  values increase from the ends towards the center of the specimen (smaller cross section). The highest values are found in the  $105^\circ$  position. The circumferential positions  $180^\circ$ - $300^\circ$  do not show significant changes. The envelopes of the circumferential positions at  $0^\circ$ - $105^\circ$  are shown in two graphs in Fig. 9 for the axial positions -5 to 0 mm (left) and 0 to 5 mm (right). In the  $0^\circ$  circumferential position, the peak position is approximately 0.15 V, with low peak heights (same as in S1, S2, and S3). In the  $60^\circ$  position, two peaks can be observed, with peak positions of 0.15 V and 0.4 V

for the first and second peaks, respectively. The peak height of the second peak is greater in the zero-axial position. The same behavior is observed in the 90° position. In this position, the first peak is not greatly altered compared to the second peak, which has higher amplitudes. It seems that the first peak is hidden due to the growth of the second peak, but some differences between the first and the second can be observed for the axial positions furthest from the center of the specimen. It can also be noted that the peak position of the second peak was shifted to lower values compared to the 0° circumferential position. The 105° position presents the highest values of the second peak, with peak positions of approximately between 0.25-0.35 V for different axial positions.

[Fig. 8 about here.]

[Fig. 9 about here.]

[Fig. 10 about here.]

### C. Optical Microscopy and XRD after fatigue

The highest  $MBN_{RMS}$  values were found in specimen S4 at the zero-axial position. In addition, because of the configuration of the fatigue test, the martensitic transformation is expected to occur initially in regions near the surface and subsurface of the specimen at the zero-axial position. Thus, in the metallographic analyses, these regions were observed. In this sense, S4 was cut cross-sectionally at the zero-axial position, and, after metallographic preparations, they were observed with the optical light microscope in the regions near the specimen surface. Figs. 10a and b correspond to different regions near the S4 surface. Fig. 10a corresponds to a region with lower MBN signals (approximately 300° circumferential position) and Fig. 10b corresponds to a region with higher MBN signals (approximately 105° circumferential position). The difference between the figures can be clearly observed. Fig. 10a does not show large changes compared to the as-received condition (Fig. 6a). The darkest region in Fig. 10b corresponds to the  $\alpha'$ -martensite formed during the fatigue test.

The XRD analyses were performed for the specimens S1 and S4 cut cross-sectionally at the zero-axial position. Fig. 11 shows the results of the XRD. In S1, only austenite peaks are observed. It is believed that small amounts of delta ferrite in the initial condition cannot be detected by XRD because of the high background noise of the XRD results. S4 was analyzed in regions close to the 105° circumferential position, but it was not possible to analyze it in regions that were very close to the surface (metallographic analysis regions). For this reason, very small peaks corresponding to  $\alpha'$ -martensite were generated.

[Fig. 11 about here.]

## IV. DISCUSSION

The MBN signals obtained in the specimens may be correlated with two types of magnetic phases present in the material: i) the  $\delta$ -ferrite and ii) the strain-induced  $\alpha'$ -martensite formed during the fatigue tests. The small MBN variations in

S1, with a peak position of 0.15 V for the measurement conditions, can be attributed to  $\delta$ -ferrite, which is the ferromagnetic phase that can be present in the as-received condition, as shown in the micrographs of Fig. 6. The small amplitudes of the MBN signal occur because of the small amounts of delta ferrite in the material.

The peak position of the MBN profile is a parameter sensitive to the hardness of the materials [18]. Ferromagnetic phases with greater hardness have higher peak positions than the softer ones [19]. Therefore, the peak position can be an indicator of which ferromagnetic phase is present in the material. The variations of Barkhausen signals in specimens S2 and S3 can also be attributed to the delta ferrite, because they have the same peak position as S1 (attributed to the delta ferrite by the measurement conditions). This assumption is consistent with the  $MBN_{RMS}$  mapping of Fig. 7. The  $MBN_{RMS}$  amplitudes are similar for the specimens S1, S2, and S3, and no higher MBN amplitudes were found near the zero-axial position in S2 and S3, where the martensitic transformation is supposed to occur first. Because the loads used were low, one can assume that the cumulative plastic deformations necessary for the martensitic transformation were not reached for specimens S2 and S3. Thus, the difference of the  $MBN_{RMS}$  distribution between the specimens S1, S2, and S3 observed in Fig. 7 occurs because of the difference in the distribution of the delta ferrite phase between the specimens.

The MBN signals for the specimen S4 at zero-axial position are consistent with the micrographs observed in Fig. 10. The highest and lowest amplitudes of MBN were found in the regions with and without martensite, respectively. Therefore, it is assumed that high  $MBN_{RMS}$  amplitudes in the other regions of S4 occur because of the presence of  $\alpha'$ -martensite in these regions. Two peaks were detected in S4 in the envelope analysis (Fig. 9). Other studies have shown that the coexistence of a hard and a soft ferromagnetic phase (e.g., martensite and ferrite) can be detected in the analysis of the MBN envelope by the presence of two peaks [20], [21]. During LCF tests of the AISI 304L, Vincent et al. (2005) [16] detected two peaks in the MBN envelope analysis. The first peak was attributed to delta ferrite because: i) it is the ferromagnetic phase that can be present in the as-received state, ii) it was created with a lower peak position, and iii) its amplitude did not change significantly during the tests, which is consistent because the  $\delta$ -ferrite volumetric fraction does not change during the fatigue tests. The second peak was attributed to  $\alpha'$ -martensite because: i) it appeared during the fatigue tests, after a certain number of cycles, ii) it was generated in a higher peak position and iii) the peak height increased during the fatigue tests, which is consistent with the increase of the  $\alpha'$ -volume fraction with the number of cycles. Due of the low carbon content of the  $\alpha'$  martensite, the hardness of this phase may not be so different than the hardness of the  $\delta$  ferrite. But the second peak can be also explain as a function of the density of the crystalline defects. The  $\delta$ -ferrite is CCC, with few defects and the martensite is slightly TCC (considered CCC, because of the low carbon content), but with greater crystalline dislocations. As the dislocations serve as a barrier to the movements of the magnetic domain walls, a greater

magnetic field (voltage - peak position) is needed to generate the Barkhausen events.

Considering the above, it can be stated that the first peak observed in S4, which is in the same position of the single peak observed in S1, S2, and S3, is related to the delta ferrite present in the material. The second peak can be attributed to the formation of  $\alpha'$ -martensite because: i) it appeared in this particular specimen, which was subjected to the greatest stresses and deformations during the tests, ii) it has a higher peak position than the first peak, therefore it can belong to the martensite, and iii) in particular circumferential positions ( $60^\circ$ - $150^\circ$ ), the peak height is higher at zero-axial position, in which martensite formation is expected in larger quantities. The increase of the second peak in S4 is believed to be due to the increase in the amount of transformed martensite in different regions of the specimen. This occurs because the increase in the amount of martensite generates an increase in the emission sources of the MBN, i.e., when more  $\alpha'$ -martensite is created in the austenite matrix, more domain walls are available to move, which produces higher MBN signals when the material is magnetized.

As mentioned, the MBN signal is also affected by the residual stresses in the material. The MBN is stress-sensitive even in the unloaded state because of the interaction of the domain walls (Bloch walls) with residual (internal) stress fields generated in the material [14]. Even a low carbon martensite has internal stress because of the shear nature of martensitic transformation; also, a compression stress is induced to the neighbor austenite because of a deformation to which it is submitted, since there is a volume expansion in the austenite to martensite transformation. In addition, the plastic deformation of the austenite-martensite can generate residual stresses. Another fact that can be considered is that the amplitude of the load used in specimen S4 was lower than the yield strength that is usually attributed to martensite; therefore, once the martensite is formed in fatigue, it is believed that it remains elastic with further cycles. This latter argument has also been used by Vincent et. al. [16]. Thus, only residual (internal) stresses within the martensite coming from the  $\gamma$ - $\alpha'$  transformation should be considered in the MBN signal. Nevertheless, the MBN behavior seems to be controlled by the increase in the amount of transformed martensite in different regions of the specimen, which increases the MBN emissions. This can be confirmed by the fact that the highest MBN amplitudes were found in some regions that were subjected to the highest stresses and deformations. Therefore, the MBN signals in S4 at  $60^\circ$ - $150^\circ$  circumferential positions observed in the MBN<sub>RMS</sub> mapping come from  $\delta$ -ferrite,  $\alpha'$ -martensite, and the influence of residual stresses, which are mostly controlled by the amount of  $\alpha'$ -martensite transformed.

The distribution (mapping) of the MBN<sub>RMS</sub> parameter shown in Fig. 8 presented an unexpected behavior; the  $\alpha'$ -martensitic transformation occurred only in particular circumferential positions. Because of the configuration of the fatigue tests, a more homogeneous distribution of the martensite was expected along each circumferential position for each axial position. Similar results were also observed by Man et. al. [22] where the strain induced martensite transformation were

not distributed homogeneously through the section of gauge parts of cyclically strained specimens. That was attributed to the chemical heterogeneities in the material generated in the manufacturing process that could have influenced in the strain induced martensitic transformation. The above could be a reason for the heterogeneous distribution of the  $\alpha'$  martensite in our results. Anyway, this region may be related to the region of greatest damage to the material. In a rotating-bending fatigue test, the specimen does not break homogeneously throughout the circumference. The damage begins somewhere on the surface of the material, giving rise later to the nucleation of the crack. Therefore, the MBN technique may be previously detecting the nucleation position of the cracks that are directly related to regions with greater martensitic transformation. To confirm this, fatigue tests until material failure must be performed to verify if the crack nucleation corresponds to the region where there was initially the greatest amount of martensite during the fatigue tests.

## V. CONCLUSION

Measurements of Magnetic Barkhausen Noise have been carried out on AISI 304L stainless steel specimens with different fatigue conditions to detect the  $\alpha'$ -martensitic transformation generated in HCF. In each specimen, MBN measurements were made at different points around the smallest cross section of the hourglass-type specimen, where fatigue damage is greater. MBN mapping allowed us to detect heterogeneities in the studied material. Knowing the characteristics of the material under study, the analysis of the MBN peaks allowed a rapid detection of the different ferromagnetic phases present in the material. The specimens subjected to loads near the fatigue limit did not show large changes in the MBN signal compared to the specimen assumed as initial condition, i.e., there was no  $\alpha'$ -martensitic transformation and only  $\delta$ -ferrite was detected. Only the specimen subjected to the greatest load showed large changes in the MBN signal, which is indirectly related to the transformed  $\alpha'$ -martensite. These were confirmed with optical micrographs and XRD analysis.

The results of this study show that the MBN technique has the potential to be a method to detect the strain-induced  $\alpha'$ -martensite in high-cycle fatigue tests, and therefore can be used as a nondestructive technique to evaluate fatigue damage in metastable austenitic stainless steels. For more accurate results, more fatigue tests under the same conditions and the study of the influence of residual stress in the fatigued specimens must be performed.

## ACKNOWLEDGMENT

The authors thank Villares Metals S. A. (Brazil) for providing the fatigue specimens and performing the fatigue tests; the Fund for the Support to Research and Extension of University of Campinas (FAEPEX) (Conv. 519.292 Corr. 1424/2015); the Don Carlos Antonio López Scholarship of Paraguay (BCAL02-189, Contract no. 22/2016); the Brazilian Nanotechnology National Laboratory (LNNano) of CNPEM for the use of the X-ray diffraction equipment; and Espaço da Escrita – Pró-Reitoria de Pesquisa – UNICAMP for the language services.

## REFERENCES

- [1] F. Grijalba and L. Padovese, "Non-destructive flaw mapping of steel surfaces by the continuous magnetic barkhausen noise method: Detection of plastic deformation," *Journal of Nondestructive Evaluation*, vol. 37, pp. 06 2018.
- [2] D. Jiles, "Dynamics of domain magnetization and the barkhausen effect," *Czechoslovak Journal of Physics*, vol. 50, no. 8, pp. 893–924, 2000.
- [3] D. Ye, Y. Xu, L. Xiao, and H. Cha, "Effects of low-cycle fatigue on static mechanical properties, microstructures and fracture behavior of 304 stainless steel," *Materials Science and Engineering: A*, vol. 527, no. 16–17, pp. 4092–4102, 2010.
- [4] G. Olson and M. Cohen, "A mechanism for the strain-induced nucleation of martensitic transformations," *Journal of the Less Common Metals*, vol. 28, no. 1, pp. 107–118, 1972.
- [5] M. Bayerlein, H.-J. Christ, and H. Mughrabi, "Plasticity-induced martensitic transformation during cyclic deformation of aisi 304l stainless steel," *Materials Science and Engineering: A*, vol. 114, pp. L11–L16, 1989.
- [6] K. Tsuzaki, T. Maki, and I. Tamura, "Kinetics of  $\alpha'$ -martensite formation during fatigue deformation in metastable austenitic stainless steel," *Le Journal de Physique Colloques*, vol. 43, no. C4, pp. C4–423, 1982.
- [7] L. Vincent, J.-C. Le Roux, and S. Taheri, "On the high cycle fatigue behavior of a type 304l stainless steel at room temperature," *International Journal of Fatigue*, vol. 38, pp. 84–91, 2012.
- [8] J. Colin, A. Fatemi, and S. Taheri, "Fatigue behavior of stainless steel 304l including strain hardening, prestraining, and mean stress effects," *Journal of Engineering Materials and Technology*, vol. 132, no. 2, p. 021008, 2010.
- [9] M. Grosse, M. Niffenegger, and D. Kalkhof, "Monitoring of low-cycle fatigue degradation in x6crniti18-10 austenitic steel," *Journal of nuclear materials*, vol. 296, no. 1, pp. 305–311, 2001.
- [10] U. Krupp, C. West, and H.-J. Christ, "Deformation-induced martensite formation during cyclic deformation of metastable austenitic steel: Influence of temperature and carbon content," *Materials Science and Engineering: A*, vol. 481, pp. 713–717, 2008.
- [11] M. Lang, J. Johnson, J. Schreiber, G. Dobmann, H.-J. Bassler, D. Eifler, R. Ehrlich, and U. Gampe, "Cyclic deformation behaviour of aisi 321 austenitic steel and its characterization by means of htc-squid," *Nuclear Engineering and Design*, vol. 198, no. 1–2, pp. 185–191, 2000.
- [12] M. Niffenegger and H. Leber, "Sensitivity of the magnetization curves of different austenitic stainless tube and pipe steels to mechanical fatigue," *Journal of Nuclear Materials*, vol. 377, no. 2, pp. 325–330, 2008.
- [13] D. O'sullivan, M. Cotterell, and I. Meszaros, "The characterisation of work-hardened austenitic stainless steel by ndt micro-magnetic techniques," *NDT & E International*, vol. 37, no. 4, pp. 265–269, 2004.
- [14] P. Haušild, K. Kolařík, and M. Karlík, "Characterization of strain-induced martensitic transformation in a301 stainless steel by barkhausen noise measurement," *Materials & Design*, vol. 44, pp. 548–554, 2013.
- [15] S. P. Sagar, B. R. Kumar, G. Dobmann, and D. K. Bhattacharya, "Magnetic characterization of cold rolled and aged aisi 304 stainless steel," *Ndt & E International*, vol. 38, no. 8, pp. 674–681, 2005.
- [16] A. Vincent, L. Pasco, M. Morin, X. Kleber, and M. Delnondedieu, "Magnetic barkhausen noise from strain-induced martensite during low cycle fatigue of 304l austenitic stainless steel," *Acta Materialia*, vol. 53, no. 17, pp. 4579–4591, 2005.
- [17] A. L. Schaeffler, "Constitution diagram for stainless steel weld metal," *Metal progress*, vol. 56, pp. 680–680B, 1949.
- [18] F. A. Franco, M. F. R. González, M. F. de Campos, and L. R. Padovese, "Relation between magnetic barkhausen noise and hardness for jominy quench tests in sae 4140 and 6150 steels," *Journal of Nondestructive Evaluation*, vol. 32, no. 1, pp. 93–103, 2013.
- [19] O. Saquet, J. Chicois, and A. Vincent, "Barkhausen noise from plain carbon steels: analysis of the influence of microstructure," *Materials Science and Engineering: A*, vol. 269, no. 1, pp. 73–82, 1999.
- [20] R. Baldev, T. Jayakumar, V. Moorthy, and S. Vaidyanathan, "Characterisation of microstructures, deformation, and fatigue damage in different steels using magnetic barkhausen emission technique," *Russian journal of nondestructive testing*, vol. 37, no. 11, pp. 789–798, 2001.
- [21] X. Kleber, A. Hug, J. Merlin, and M. Soler, "Ferrite-martensite steels characterization using magnetic barkhausen noise measurements," *ISIJ international*, vol. 44, no. 6, pp. 1033–1039, 2004.
- [22] J. Man, M. Smaga, I. Kuběna, D. Eifler, and J. Polák, "Effect of metallurgical variables on the austenite stability in fatigued aisi 304 type steels," *Engineering Fracture Mechanics*, vol. 185, pp. 139 – 159, 2017, xviii International Colloquium Mechanical Fatigue of Metals.



**Roberto M. Giménez Cáceres** was born in Paraguay in 1990. He received his Electromechanical Engineering degree from the School of Engineering of the National University of Asunción, Paraguay, in 2015, and his Master Degree from the School of Mechanical Engineering of the University of Campinas, Brazil, in 2018. His main area of interest is the use of the Magnetic Barkhausen Noise as a non-destructive technique.

**Freddy A. Franco Grijalba** was born in Colombia in 1976. He received his Mechanical Engineering degree from the University of Ibagué, Colombia, in 2001, and his Doctoral degree from the School of Engineering of the University of São Paulo, Brazil, in 2010. He is a Full Professor in the Department of Mechanical Engineering of the University of Campinas, Brazil, since 2014. His main areas of interest are ultrasonic characterization of elastic solids, and development of new applications of the Magnetic Barkhausen Noise technique.

**Paula Fernanda da Silva Farina** was born in Brazil in 1978. She received her Metallurgical Engineering degree from Ignatian Educational Foundation – FEI, in 2003, and her Master and Doctoral Degree from the School of Engineering of the University of São Paulo, Brazil, in 2006 and 2011, respectively. She is a Full Professor in the Department of Manufacturing and Materials of the University of Campinas, Brazil, since 2015. Her main areas of interest are phase transformations and characterization of metallic materials.

LIST OF FIGURES

|    |  |    |
|----|--|----|
| 1  | Barkhausen noise signal and its Envelope with magnetizing voltage as a function of time. . . . .   | 8  |
| 2  | Schematic of fatigue specimens (dimensions in mm). . . . .   | 9  |
| 3  | Schematic of the experimental set-up used for MBN measurements. . . . .  | 10 |
| 4  | Points for MBN measurements. . . . .   | 11 |
| 5  | Schematic representation of the bending moment and stress distribution in an hour-glass type specimen under rotating bending loads. . . . .  | 12 |
| 6  | Optical micrograph of the AISI 304L steel showing austenitic grains and islands of delta ferrite for the material cut in the a) transversal and b) longitudinal direction. . . . . | 13 |
| 7  | MBN <sub>RMS</sub> distribution and envelopes from the regions of highest MBN <sub>RMS</sub> values of the: a) S1, b) S2 and c) S3 sample. . . . .                                 | 14 |
| 8  | MBN <sub>RMS</sub> distribution of the S4 sample. . . . .  | 15 |
| 9  | Envelopes of the 0°-105° circumferential positions of the S4 sample for the -5 to 0 mm (left) and, 0 to 5 mm (right) axial position. . . . .                                       | 16 |
| 10 | Light micrography near the edges of the: a) S4-300° and b) S4-105° at zero-axial position. . . . .   | 17 |
| 11 | XRD of the S1 and S4 samples. . . . .  | 18 |

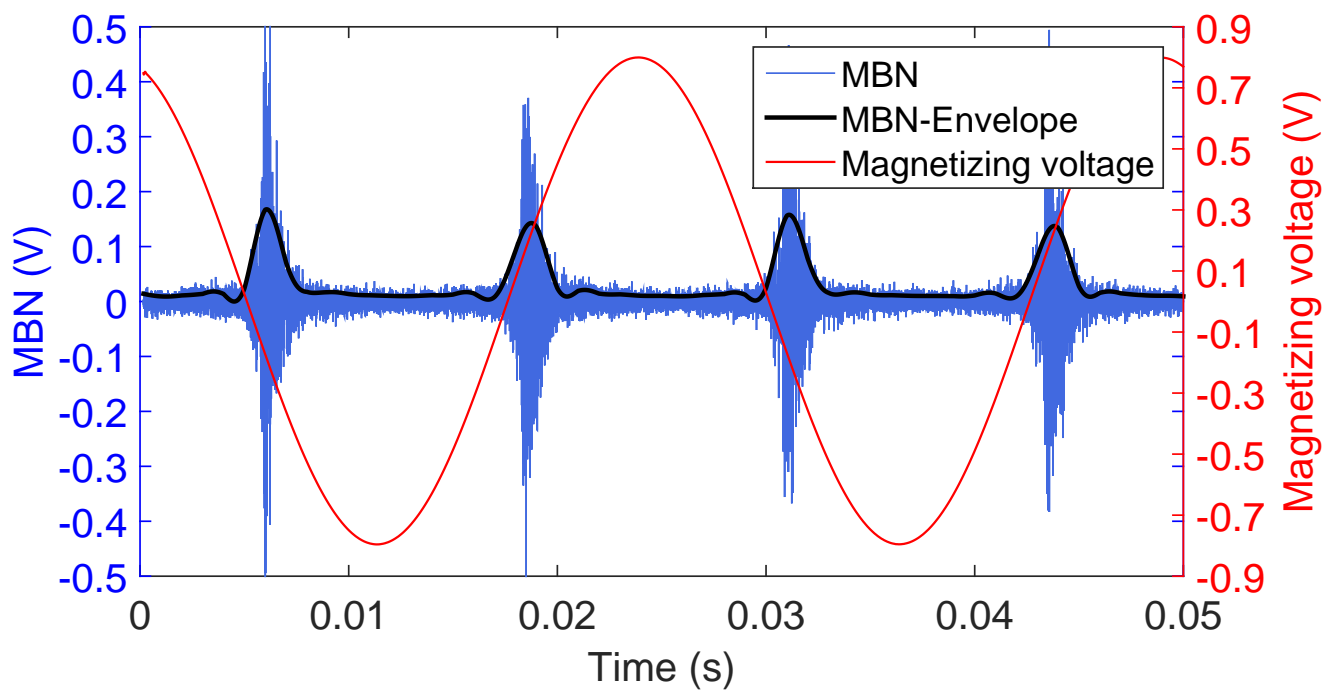


Fig. 1. Barkhausen noise signal and its Envelope with magnetizing voltage as a function of time.

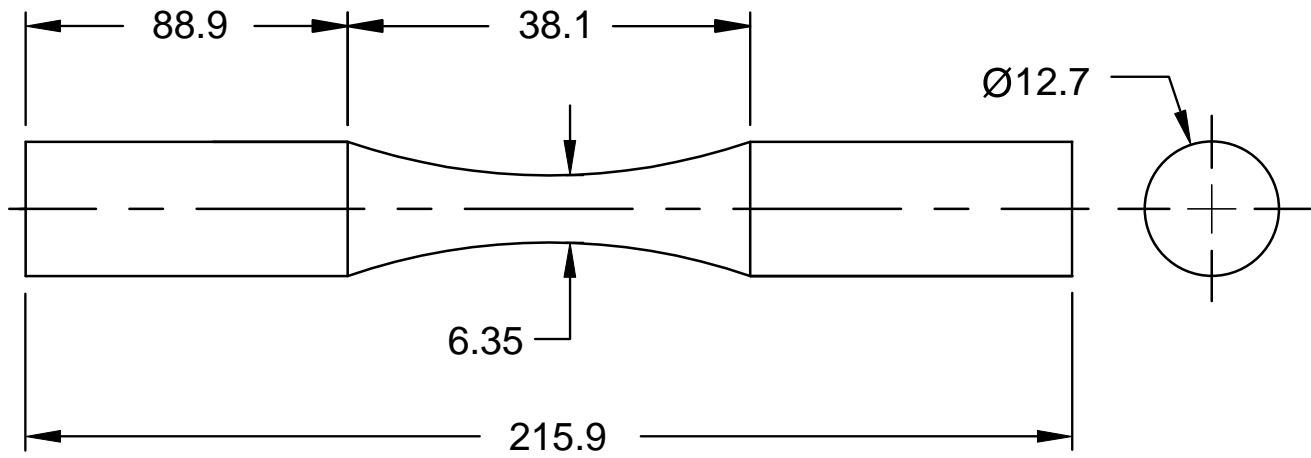


Fig. 2. Schematic of fatigue specimens (dimensions in mm).

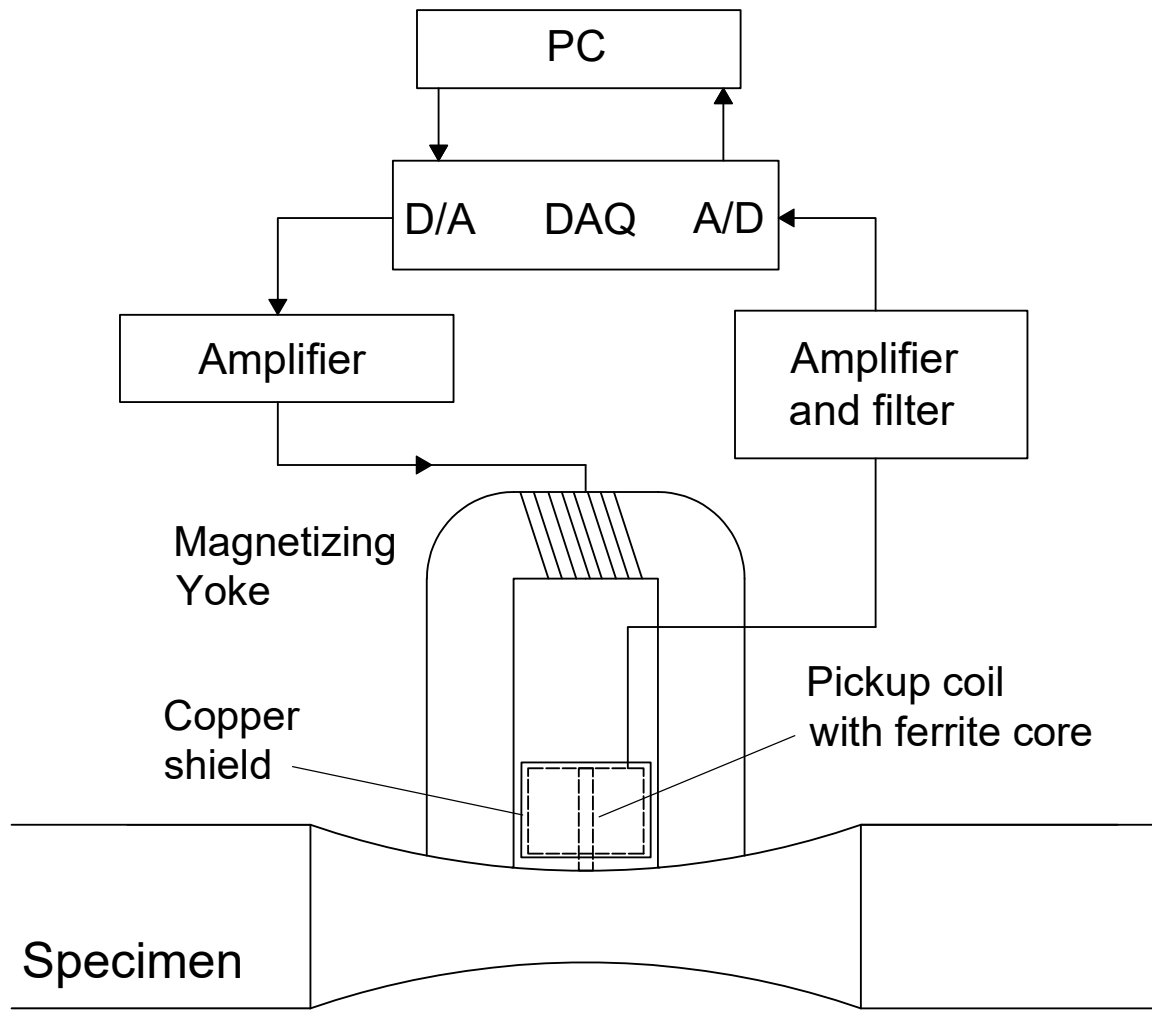


Fig. 3. Schematic of the experimental set-up used for MBN measurements.

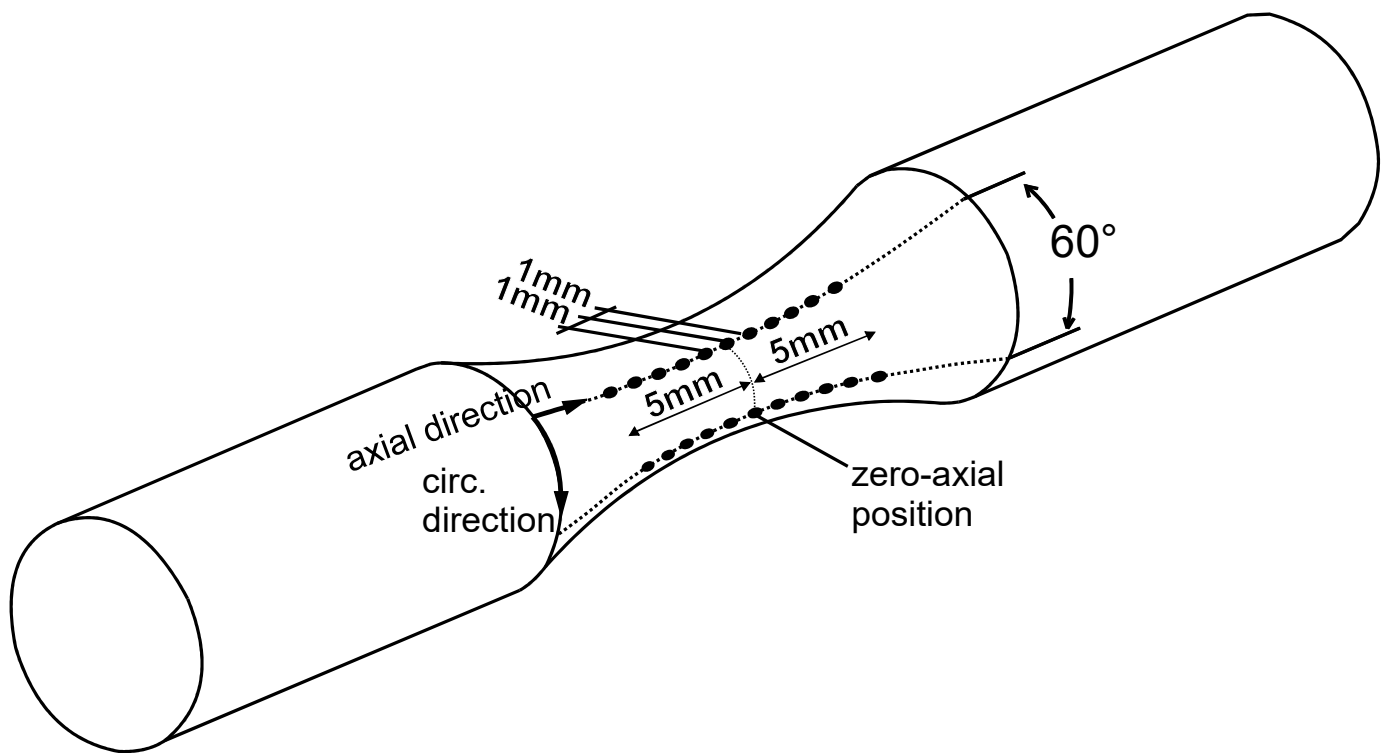


Fig. 4. Points for MBN measurements.

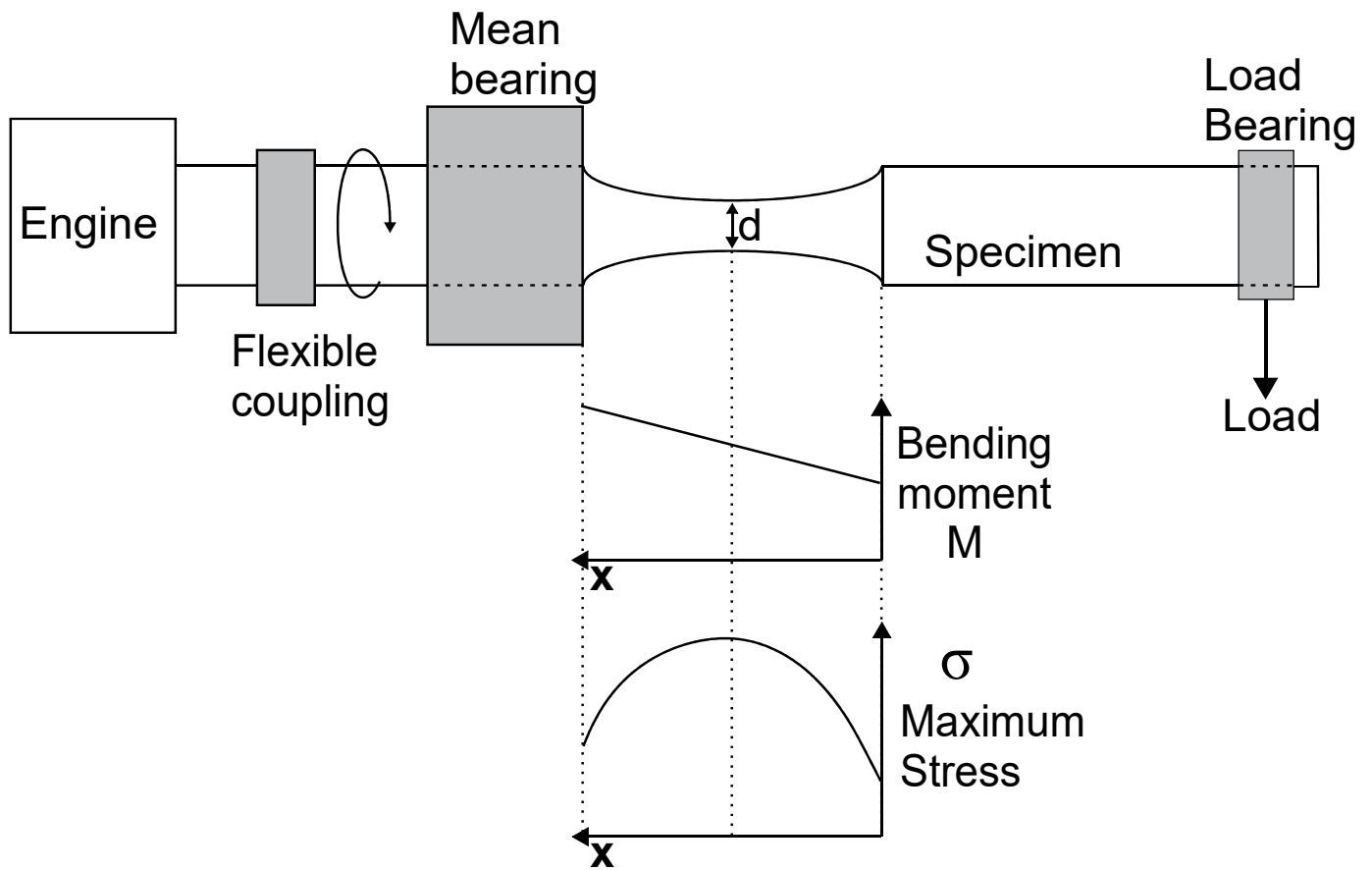


Fig. 5. Schematic representation of the bending moment and stress distribution in an hour-glass type specimen under rotating bending loads.

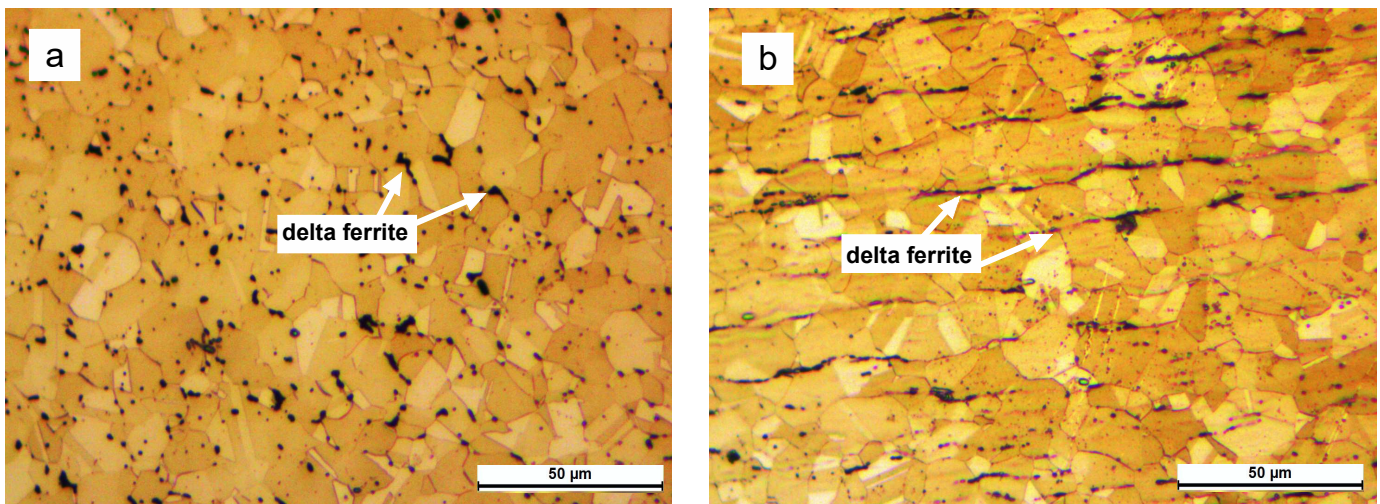


Fig. 6. Optical micrograph of the AISI 304L steel showing austenitic grains and islands of delta ferrite for the material cut in the a) transversal and b) longitudinal direction.

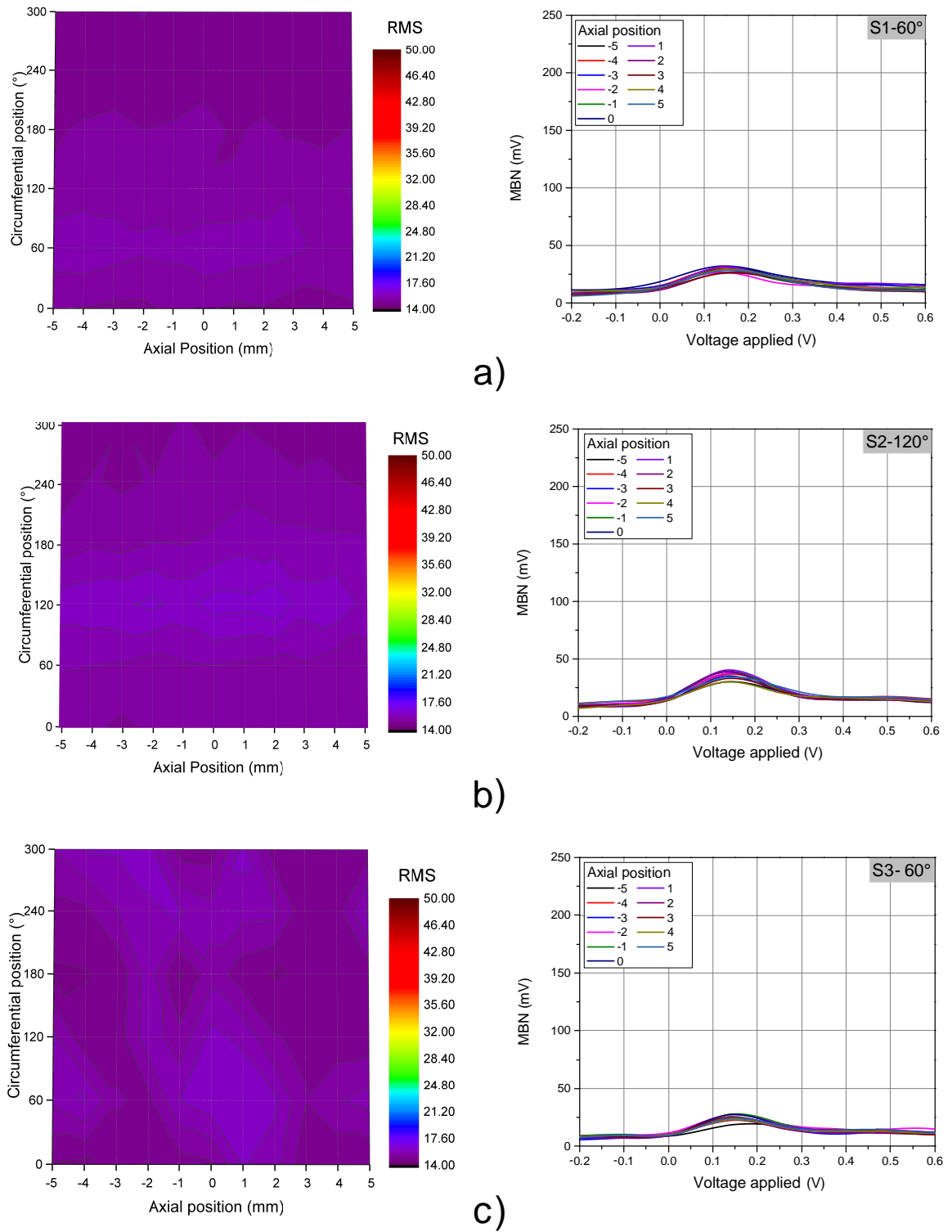


Fig. 7. MBN<sub>RMS</sub> distribution and envelopes from the regions of highest MBN<sub>RMS</sub> values of the: a) S1, b) S2 and c) S3 sample.

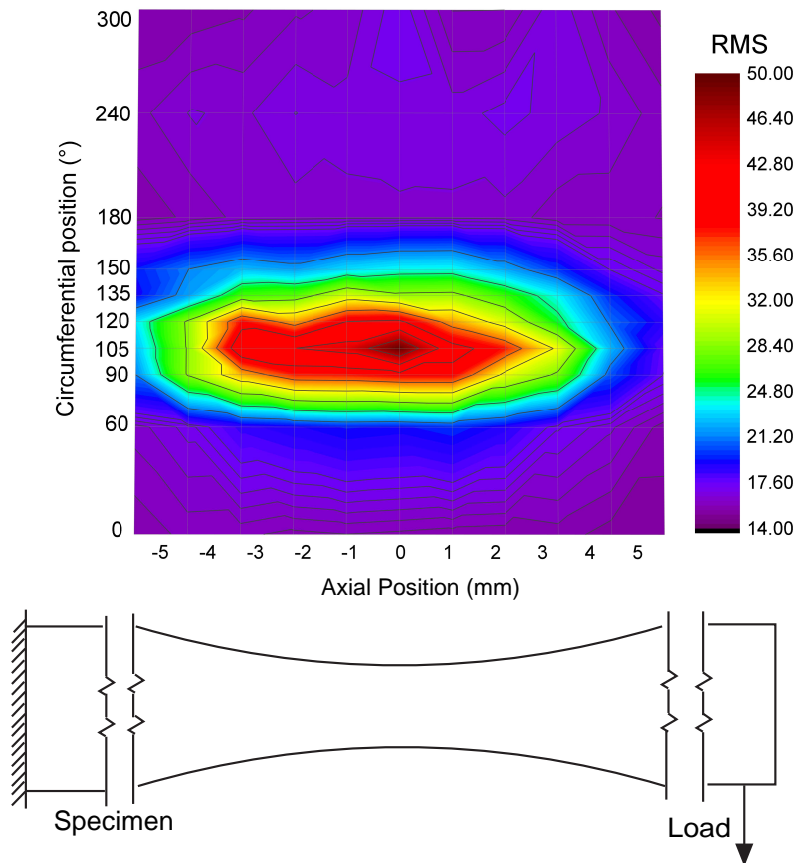


Fig. 8. MBN<sub>RMS</sub> distribution of the S4 sample.

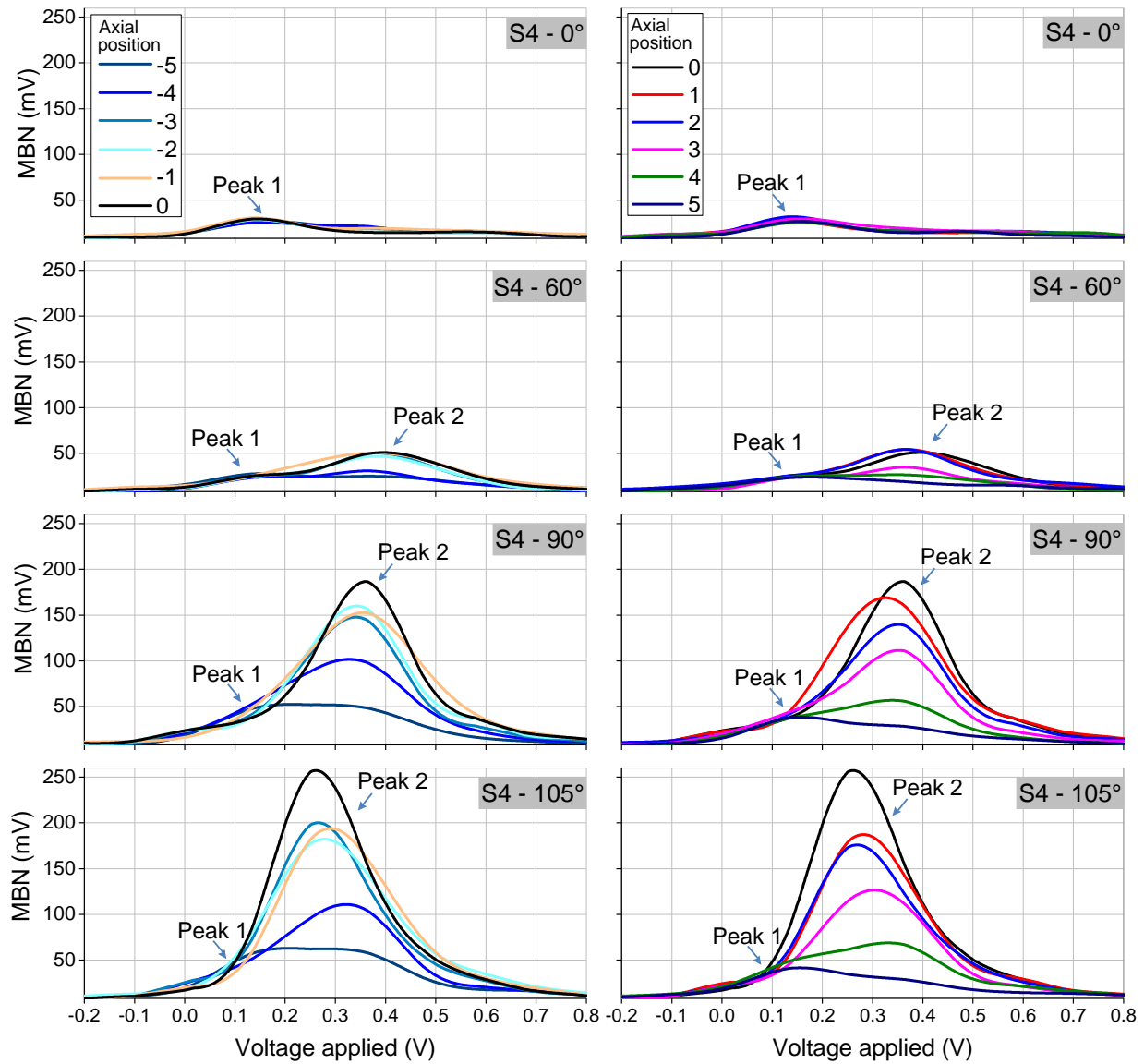


Fig. 9. Envelopes of the 0°-105° circumferential positions of the S4 sample for the -5 to 0 mm (left) and, 0 to 5 mm (right) axial position.

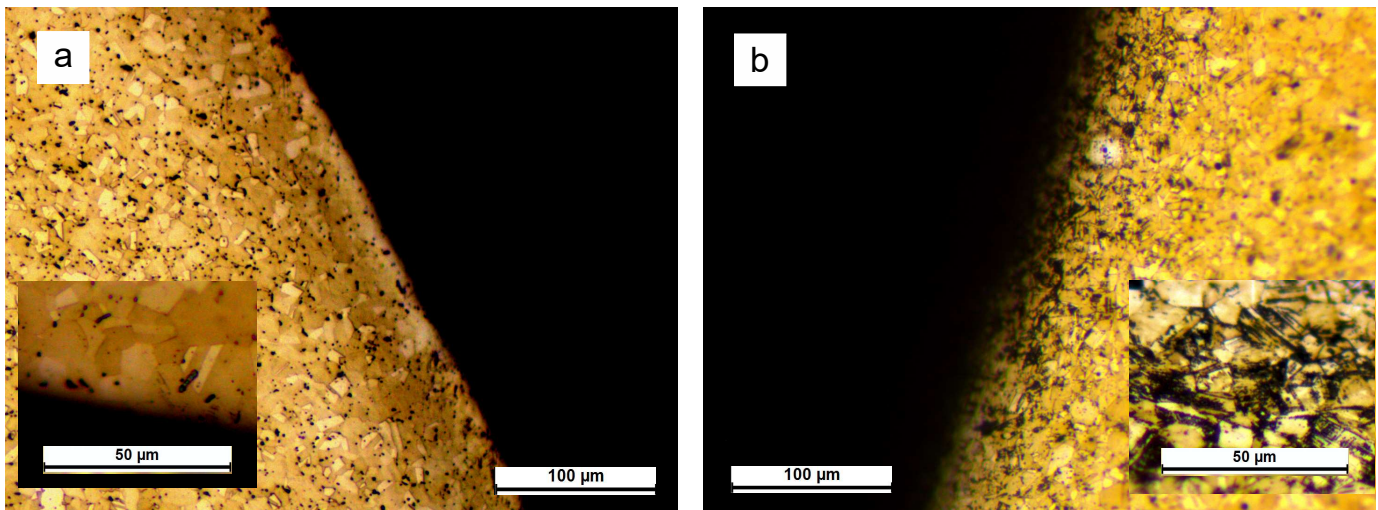


Fig. 10. Light micrography near the edges of the: a) S4-300° and b) S4-105° at zero-axial position.

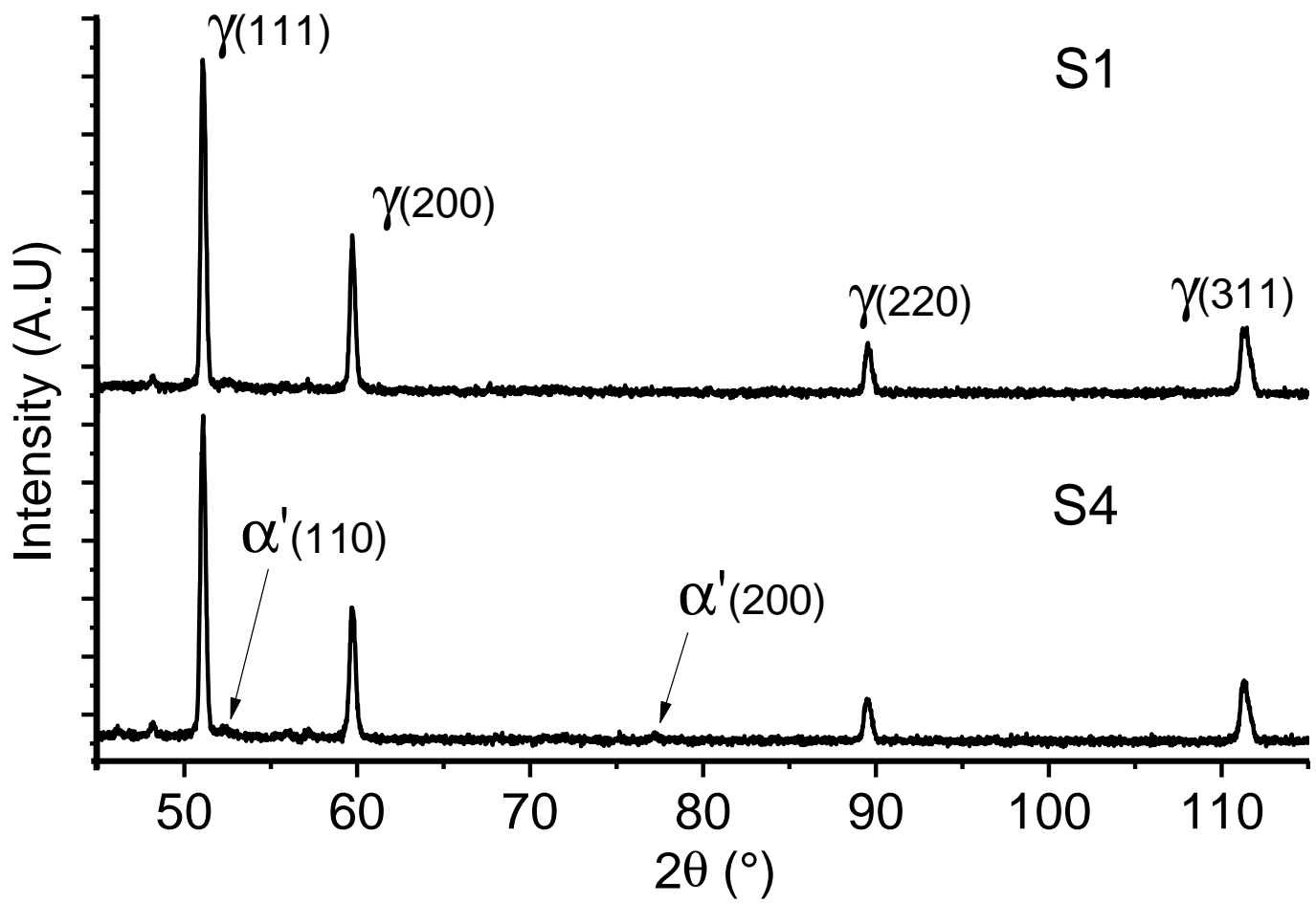


Fig. 11. XRD of the S1 and S4 samples.

LIST OF TABLES

|     |   |    |
|-----|---|----|
| I   | Mechanical properties of AISI 304L steel. . . . .       | 20 |
| II  | Chemical composition of AISI 304L steel . . . . .       | 21 |
| III | Load and number of cycles for fatigue testing . . . . . | 22 |

TABLE I  
MECHANICAL PROPERTIES OF AISI 304L STEEL.

| Ultimate tensile stress, $\sigma_{uts}$ (MPa) | Yield stress, $\sigma_{ys}$ (MPa) | Brinell Hardness HB |
|---|-----------------------------------|---------------------|
| 520   | 220                               | 160                 |

TABLE II  
CHEMICAL COMPOSITION OF AISI 304L STEEL

| C     | Si   | Mn   | P     | S     | Co   | Cr    | Mo   | Ni   | V    | W    | Cu   | Ti    | Nb   | Al    | N      | O      |
|-------|------|------|-------|-------|------|-------|------|------|------|------|------|-------|------|-------|--------|--------|
| 0.024 | 0.19 | 1.83 | 0.038 | 0.023 | 0.15 | 18.18 | 0.63 | 8.21 | 0.05 | 0.09 | 0.33 | 0.005 | 0.01 | 0.005 | 0.0981 | 0.0128 |

TABLE III  
LOAD AND NUMBER OF CYCLES FOR FATIGUE TESTING

| Sample | Calculated maximum stress (MPa) | Testing cycle     | Theoretical number of cycles for failure |
|--------|---------------------------------|-------------------|--|
| S1     | 0                               | 0                 | -  |
| S2     | 200                             | $> 3 \times 10^7$ | $\infty$                                 |
| S3     | 240                             | $5 \times 10^5$   | $7 \times 10^5$                          |
| S4     | 270                             | $1.5 \times 10^5$ | $2 \times 10^5$                          |